Real photon structure at an e^+e^- linear collider

Andreas Vogt[a*]

[a]Instituut-Lorentz, University of Leiden, P.O. Box 9506, 2300 RA Leiden, The Netherlands

Previous studies of the kinematic coverage for measuring the photon structure function F_2^γ at a future 500 GeV e^+e^- linear collider [1,2] are updated using current estimates of luminosities and important detector parameters. The perturbative expansion for the evolution of F_2^γ is briefly recalled in view of a recent claim [3] that all existing next-to-leading order analyses of the photon structure are incorrect. A simple illustration is given of the different sensitivities of hadronic and photonic structure functions on the strong coupling constant α_s.

1. KINEMATICS

The basic kinematics of electron-photon ($e\gamma$) deep-inelastic scattering (DIS) at an e^+e^- or e^-e^- collider is recalled in Fig. 1. Here and in what follows we consider only the electromagnetic one-photon-exchange process, i.e., it is assumed that QED radiative corrections and contributions due to the exchange of weak gauge bosons have been subtracted. For a recent study of neutral- and charged-current processes see ref. [4].

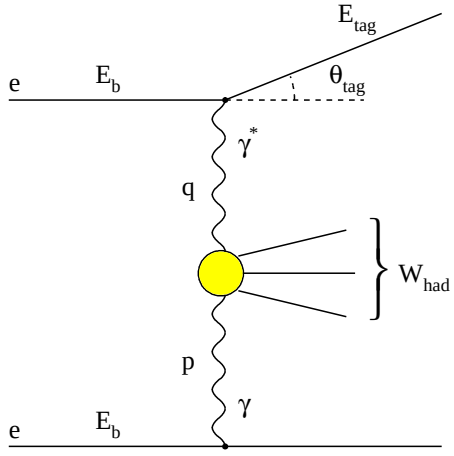

Figure 1. The kinematics of inclusive electromagnetic electron scattering off (quasi-)real photons in e^+e^- or e^-e^- collisions.

*Work supported by the EC network 'QCD and Particle Structure' under contract No. FMRX–CT98–0194.

The unpolarised $e\gamma$ DIS cross section is, at lowest order in the electromagnetic coupling α,

$$\frac{d\sigma(e\gamma \to eX)}{dE_{\rm tag}\, d\cos\theta_{\rm tag}} = \frac{4\pi\alpha^2 E_{\rm tag}}{Q^4 y} \cdot \Big[\big\{1+(1-y)^2\big\}F_2^\gamma(x,Q^2) - y^2 F_L^\gamma(x,Q^2)\Big] . \quad (1)$$

Here $F_{2,L}^\gamma(x,Q^2)$ denote the structure functions of the real photon. The virtuality of the probing photon and the invariant mass of the hadronic final state are given by

$$\begin{aligned} Q^2 &\equiv -q^2 = 2E_b E_{\rm tag}(1-\cos\theta_{\rm tag}) , \\ W_{\rm had}^2 &= (q+p)^2 . \end{aligned} \quad (2)$$

The scaling variables x and y read

$$\begin{aligned} x &= \frac{Q^2}{Q^2+W_{\rm had}^2} , \\ y &= 1 - \frac{E_{\rm tag}}{E_b}\cos^2\left(\frac{\theta_{\rm tag}}{2}\right) . \end{aligned} \quad (3)$$

The measured cross section is obtained by convoluting Eq. (1) with the flux $f_{\gamma,e}(z = E_\gamma/E_{\rm beam})$ of the incoming (quasi-)real photons.

If the photon momentum p is known, then not only Q^2 and y, but also $W_{\rm had}$ and x in Eqs. (2) and (3) are fixed by energy and angle of the 'tagged' outgoing electron, as in usual electron-proton DIS. If p is unknown, the determination of x has to proceed via calorimetric measurements of the hadronic final state. Beam-pipe losses then render it very difficult, if not impossible, to obtain high-precision data on $F_2^\gamma(x,Q^2)$.

2. PHOTON SPECTRA

A ubiquitous source of quasi-real photons at an electron collider is the soft bremsstrahlung ('Weizsäcker-Williams') spectrum emitted by almost undeflected electrons [5]. This spectrum has been the photon source for the F_2^γ measurements at LEP and previous e^+e^- colliders [6], where the corresponding electrons are undetected ('anti-tagged'). In order to determine the momenta of the quasi-real photons, however, as required for precision measurements of F_2^γ, these forward electrons need to be tagged as well. Due to the high beam energies E_b at a linear collider this should be done at angles $\theta_f \lesssim 2$ mrad, restricting the high-virtuality tail of the WW spectrum which reaches up to $P^2 \equiv -p^2 \simeq (1-z)\,E_b^2\,\theta_f^2$. It seems not too likely that this can be achieved with high accuracy and efficiency.

For an optimistic estimate of possible event numbers in this scenario we will assume a 10% efficiency for $0.2\,E_b \le x \le 0.8\,E_b$. Thus we use

$$f_{\gamma/e}^{\rm WW}(z) = K\,\theta(z-0.2)\,\theta(0.8-z) \qquad (4)$$
$$\frac{\alpha}{\pi z}\Big[\big(1+(1-z)^2\big)\ln\frac{E_b\theta_f(1-z)}{m_e z} - (1-z)\Big]$$

with $K = 0.1$ and $\theta_f = 2$ mrad.

A very appealing new possibility envisaged for the linear collider is to operate the machine as an $e\gamma$ collider as well. This can be realized by converting one of the electron beams to a real-photon beam by backscattering of laser photons [7]. Subsequently the resulting broad spectrum can be transformed into a rather monochromatic photon beam,

$$E_\gamma \simeq 0.8\,E_b \;\text{ with }\; \Delta E_\gamma \approx 0.1\,E_\gamma\,, \qquad (5)$$

under suitable machine conditions, see ref. [8].

For our illustrations below we will employ a simple model spectrum [2] incorporating Eq. (5) and the rough shape of the high-z peak:

$$f_{\gamma/e}^{\rm BL}(z) = K'\theta(z-0.63)\,\theta(0.83-z)\,375\,(z-0.63)^2 \qquad (6)$$

with $K' = 0.1$. The latter suppression factor leads to a conservative estimate of the attainable $e\gamma$ luminosity. The flux functions (4) and (6) are compared in Fig. 2.

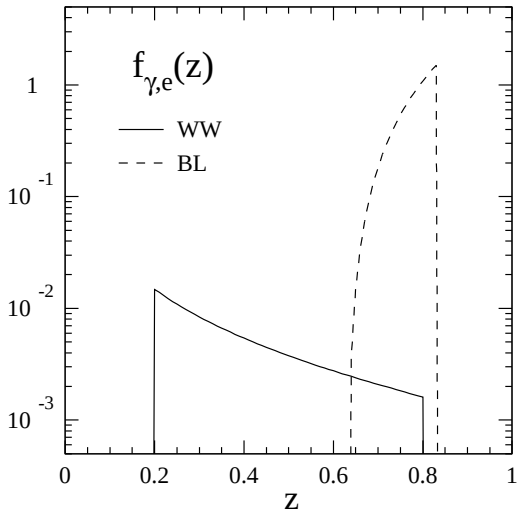

Figure 2. The effective flux functions for bremsstrahlung (WW) and backscattered laser (BL) photons given in Eq. (4) and Eq. (6), respectively.

3. EVENT NUMBERS, F_2^γ COVERAGE

The kinematic coverage for measurements of $F_2^\gamma(x,Q^2)$ strongly depends on the minimal angle $\theta_{\rm tag,min}$ down to which the scattered electron can be detected. In fact, an electron tagger inside the radiation shielding masks of the main detector at about 10 degrees is indispensable for accessing the region $Q^2 < 1000$ GeV^2 at a 500 GeV machine. Presently $\theta_{\rm tag,min} = 25$ mrad is considered feasible, a value even below the 40 mrad demanded in ref. [2]. Also important is the background suppression cut $E_{\rm tag,min}$ on the energy of the scattered electron. For the present study we replace the previous choice $0.5\,E_b$ by the weaker requirement $E_{\rm tag,min} = 50$ GeV. The accessible y-range is thus enlarged from $y \le 0.5$ to $y \le 0.8$.

The resulting event numbers are shown in Fig. 3 for the bremsstrahlung scenario (4), and in Fig. 4 for the laser backscattering scenario (6). $F_{2,L}^\gamma$ in Eq. (1) are calculated using the leading-order GRV parametrisation [9]. An integrated e^+e^- luminosity of 200 fb^{-1}, typical for the present TESLA design, is assumed. In both cases this luminosity is effectively reduced by a factor of 10 by the $f_{\gamma,e}$ assumptions in Sect. 2. Under

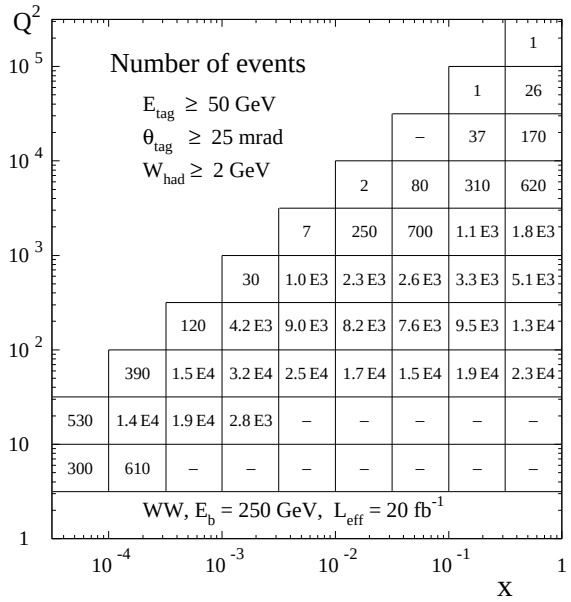

Figure 3. Expected event numbers of $e\gamma$ DIS for bremsstrahlung photons at a 500 GeV linear collider. Forward-electron tagging is assumed to be possible with 10% efficiency for $\theta_f \leq 2$ mrad and electron energies between 50 and 200 GeV.

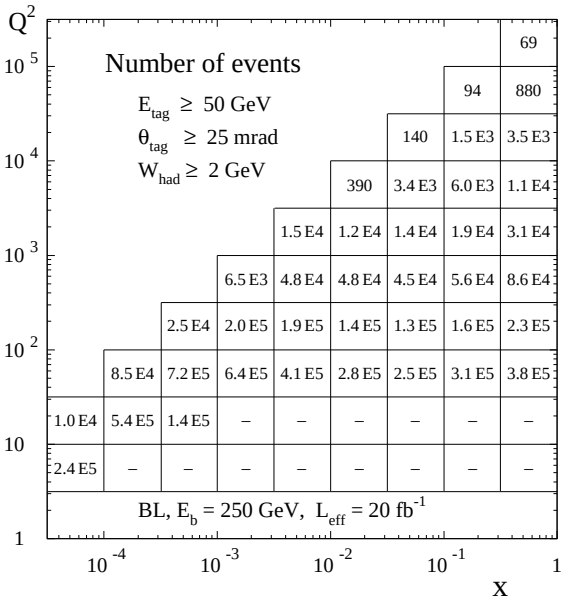

Figure 4. Expected event numbers of electron-photon DIS for the backscattered-laser $e\gamma$ mode of a 500 GeV linear collider. It is assumed that 10% of the e^+e^- luminosity can be reached in this mode for a rather monochromatic photon beam.

these conditions the $e\gamma$ collider is, as expected from Fig. 2, vastly superior to the WW scenario. E.g., the difference in the high-Q^2 reach at large x amounts to one order of magnitude.

The maximal accuracies for F_2^γ determinations are illustrated in Fig. 5 for the preferred $e\gamma$ case. Here we have assumed that the systematic error is equal to the statistical one inferred from the event numbers, but amounts to at least 3%. For the present parameters, precision measurements are possible at large x for 40 GeV$^2 \lesssim Q^2 \lesssim 10^4$ GeV^2. The region $Q^2 < 30$ GeV^2 can only be reached by a (preferably asymmetric) lower energy run. However, such Q^2-values can be accessed at very small x. Only in this region, $x \approx 10^{-4}$, the cross section (1) receives noticeable contributions from the longitudinal structure function F_L^γ.

Charm production contributes about 30–40% to the cross section over almost the entire kinematic region of Fig 4. A decent measurement of $F_2^{\rm charm}$ should thus be possible at large x, where the final-state particles are not too forward.

4. EVOLUTION OF F_2^γ

We now turn to the theoretical description of F_2^γ in perturbative QCD. For notational simplicity we restrict ourselves to the flavour non-singlet part, and consider the contributions of effectively massless quarks only (see ref. [10] for the singlet case). All functional dependences and obvious indices will be suppressed together with overall charge factors, e.g., we will write F^γ instead of $F_{2,\rm NS}^\gamma(x,Q^2)/\alpha$. It is understood that all products of x-dependent quantities have to be read as convolutions in Bjorken-x space.

In terms of a suitable combination q^γ of quark densities the non-singlet structure function reads

$$F^\gamma = C_q \, q^\gamma + C_\gamma \tag{7}$$

at lowest order in the electromagnetic coupling α. In this approximation the quark density q^γ is subject to the inhomogeneous evolution equation

$$\dot{q}^\gamma \equiv \frac{dq^\gamma}{d\ln Q^2} = k + P\, q^\gamma \tag{8}$$

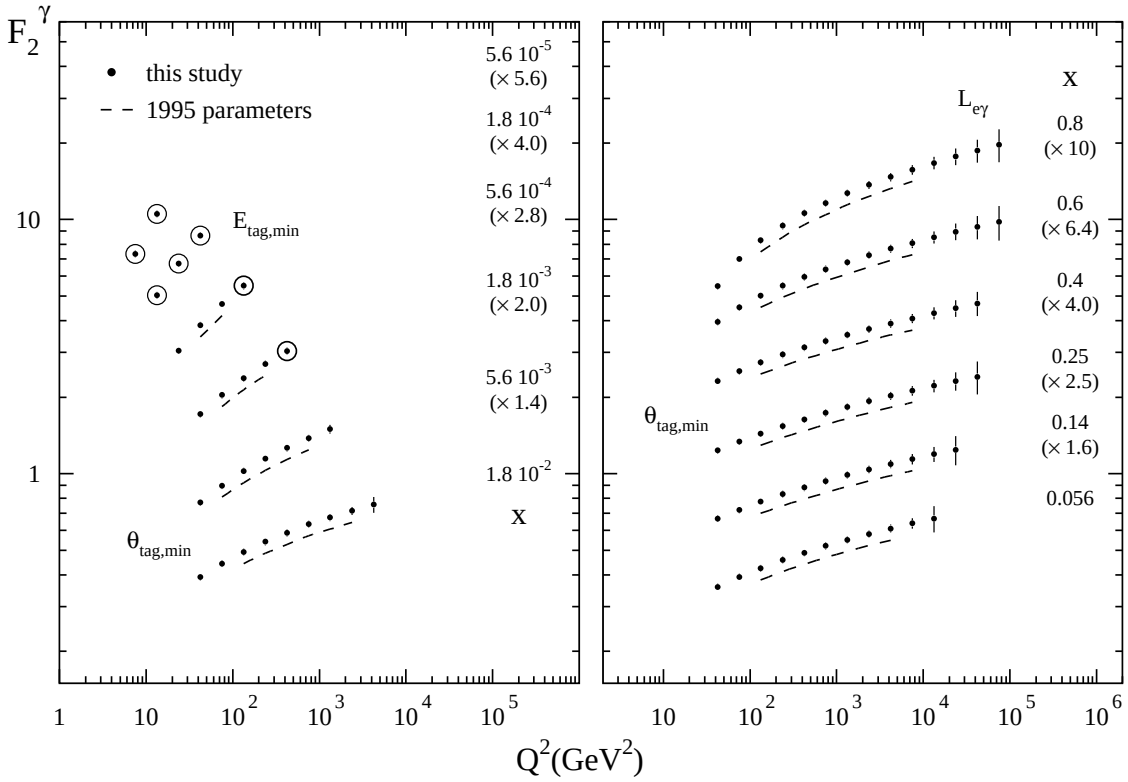

Figure 5. The possible kinematic coverage and maximal accuracy of the measurement of F_2^γ for the backscattered-laser $e\gamma$ mode at a 500 GeV linear collider. The open circles show the bins with an expected F_L^γ-effect of 10% or more. The sources of the extended x and Q^2 reach with respect to the 1995 study [2] are indicated. The values of F_2^γ have been scaled by the factors given in the figure.

for the choice $\mu_f^2 = Q^2$ of the factorization scale.

The corresponding photon and quark coefficient functions C_q and C_γ in Eq. (7) have the perturbative expansions

$$C_q = 1 + \sum_{l=1} a_s^l C_q^{(l)} \ , \quad C_\gamma = \sum_{l=1} a_s^{l-1} C_\gamma^{(l)} \tag{9}$$

in terms of the strong coupling $a_s \equiv \alpha_s/(4\pi)$. The scale dependence of a_s is governed by

$$\frac{da_s}{d\ln\mu_r^2} = \beta(a_s) = -\sum_{l=0} a_s^{l+2}\beta_l \tag{10}$$

where μ_r is the renormalization scale. Finally the non-singlet quark-quark and photon-quark splitting functions in Eq. (8) read

$$P = \sum_{l=0} a_s^{l+1} P^{(l)} \ , \quad k = \sum_{l=0} a_s^l k^{(l)} \ . \tag{11}$$

The expansion coefficients in Eqs. (9) and (11) are Q^2-independent for $\mu_r^2 = \mu_f^2 = Q^2$. They do depend, however, on the mass-factorization and renormalization schemes. While the latter dependence is unavoidable in perturbative calculations, the former can be eliminated by expressing the observable $\dot{F}^\gamma \equiv dF^\gamma/d\ln Q^2$ in terms of F^γ itself. By inserting Eq. (7) solved for q_γ into

$$\dot{F}^\gamma = \dot{C}_q \cdot q^\gamma + C_q \cdot \dot{q}^\gamma + \dot{C}_\gamma \tag{12}$$

after using Eq. (8), one arrives at

$$\begin{aligned} \dot{F}^\gamma \ &= \ \left\{ -\dot{C}_q C_q^{-1} C_\gamma + C_q k - P C_\gamma + \dot{C}_\gamma \right\} \\ &\quad + \left\{ \dot{C}_q C_q^{-1} + P \right\} F^\gamma \ . \end{aligned} \tag{13}$$

The combinations of splitting functions and coefficient functions enclosed by the brackets are scheme invariant.

Insertion of the perturbative expansions (9–11) into Eq. (13) finally yields, for $\mu_r^2 = Q^2$,

$$\begin{aligned}\dot{F}^\gamma \;=\;& a_s^0\, k^{(0)} \\ &+ a_s^1 \big\{ k^{(1)} + C_q^{(1)} k^{(0)} - P^{(0)} C_\gamma^{(1)} \big\} \\ &+ a_s^2 \big\{ k^{(2)} + C_q^{(1)} k^{(1)} + C_q^{(2)} k^{(0)} - P^{(0)} C_\gamma^{(2)} \\ &\qquad - P^{(1)} C_\gamma^{(1)} - \beta_0 C_\gamma^{(1)} - \beta_0 C_q^{(1)} C_\gamma^{(1)} \big\} \\ &+ F^\gamma \Big[a_s^1\, P^{(0)} \\ &+ a_s^2 \big\{ P^{(1)} - \beta_0 C_q^{(1)} \big\} \\ &+ a_s^3 \big\{ P^{(2)} - \beta_0 [2 C_q^{(2)} - C_q^{(1)2}] - \beta_1 C_q^{(1)} \big\} \Big] \\ &+ O(a_s^3) \;+\; F^\gamma \cdot O(a_s^4) \;. \end{aligned} \tag{14}$$

The generalization to $\mu_r^2 \neq Q^2$ can be obtained by expressing $a_s \equiv a_s(Q^2)$ as a power series in $a_s(\mu_r^2)$ via Eq. (10), inserting this expression into Eq. (14), and re-expanding the result in terms of $a_s(\mu_r^2)$ up to the same order as before for $a_s(Q^2)$. The combinations enclosed in the curved brackets in Eq. (14) are, as the leading terms $k^{(0)}$ and $P^{(0)}$, factorization scheme (and scale) invariant since the relation (14) between observables holds irrespective of the values of a_s and F^γ.

Note that $C_\gamma^{(1)}$, despite being an a_s^0-coefficient in Eq. (9), enters $\dot{F}_2^\gamma$ on the same level as the hadronic next-to-leading order (NLO) quantity $C_q^{(1)}$. Hence $C_\gamma^{(1)}$ is to be considered as a NLO contribution as well. Notice also that $k^{(1)}$, like its hadronic NLO counterpart $P^{(1)}$, is changed by a re-definition of $C_q^{(1)}$, e.g., by switching from the $\overline{\rm MS}$ or DIS$_\gamma$ schemes [11] to the DIS scheme. Correspondingly $C_\gamma^{(2)}$ and the presently uncalculated quantity $k^{(2)}$ contribute in next-to-next-to-leading order only. Looking back to Eqs. (8) and Eqs. (14) these findings imply that, for the purpose of power-counting in α_s, the quark densities q^γ and the structure function F_2^γ have to be counted as $1/\alpha_s$.

The correct counting just described is implemented in the NLO photon-structure parametrisations of refs. [9,12] and countless applications to specific processes. It is, however, in direct contradiction to ref. [3], where $C_\gamma^{(1)}$ is considered as a leading-order term and $C_\gamma^{(2)}$ and $k^{(2)}$ are claimed to be NLO quantities.

5. SENSITIVITIES ON α_s

The dependence of the large-x evolution of F_2^γ on the strong coupling constant α_s is quite different from that of hadronic structure functions. The latter case is recalled in Fig. 6 where the NLO pion parametrisation of ref. [13], after transformation to the DIS scheme at $Q^2 = 4$ GeV^2, is evolved for four flavours. The α_s-sensitive quantities are the logarithmic Q^2-slopes of F_2 at large x; an overall normalization error is irrelevant.

The corresponding results for the photon case are illustrated in Fig. 7 using the parametrisation of ref. [9]. Here the α_s-sensitive quantities are the absolute values of F_2^γ at very large-x and high Q^2, cf. ref. [14]. At $x = 0.8$, e.g., a change of $\alpha_s(M_Z)$ by 5% leads to an effect of about 3% on F_2^γ.

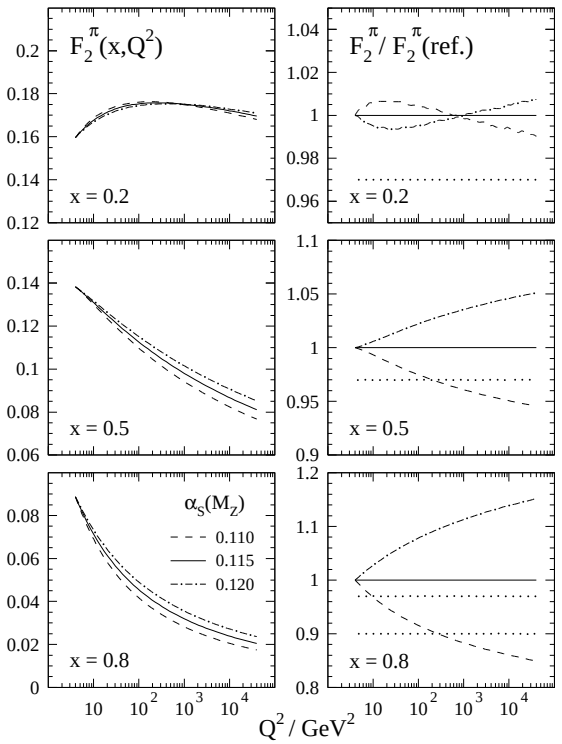

Figure 6. The α_s-dependence of the large-x NLO evolution of the neutral-pion structure function F_2^π for a fixed input at $Q^2 = 4$ GeV^2. The dotted lines show the effect of input normalization offsets of -3% and -10% on the $\alpha_s(M_Z)$=0.115 curves.

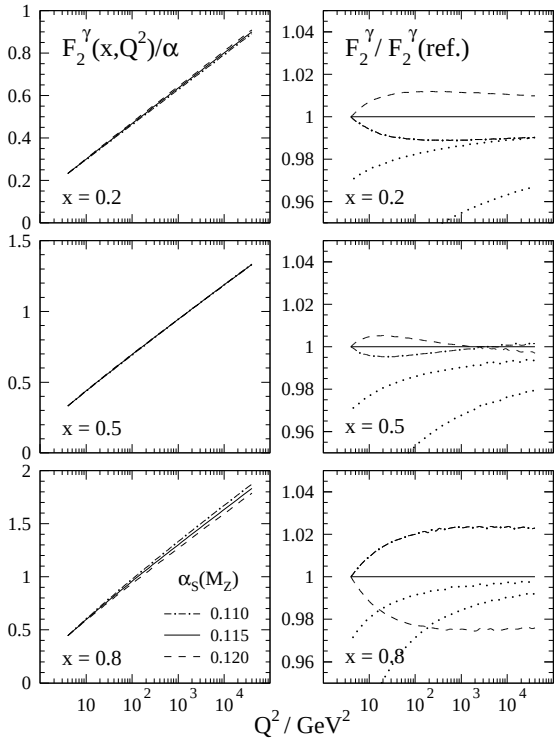

Figure 7. As Fig. 6, but for F_2^γ. Note the shrinking high-Q^2 impact of low-scale normalization changes at large x, and the almost identical shapes of the upper dotted ($\alpha_s(M_Z)$=0.115) and the dash-dotted (α_s=0.110) curves at $x = 0.8$.

6. CONCLUSIONS

A high-energy $e\gamma$ collider, realised via Compton backscattering of laser photons at a future e^+e^- collider, would be a unique source of information on the photon structure. At a 500 GeV machine the structure function F_2^γ can be accurately measured at large x for 40 GeV$^2 \lesssim Q^2 \lesssim 10^4$ GeV^2. Small values of x down to below 10^{-4} can be reached for $Q^2 \approx 10$ GeV^2, thus complementing the F_2^p results of HERA in this regime.

At large values of x and Q^2, $x > 0.7$ and $Q^2 > 10^3$ GeV^3, the absolute values of F_2^γ become robust predictions of perturbative QCD. A competitive extraction of α_s from these values would require very high accuracies on both the experimental and the theoretical sides.

ACKNOWLEDGMENT

It is a pleasure to thank A. de Roeck for discussions on detector parameters and final-state cuts for electron-photon DIS at the linear collider.

REFERENCES

1. D.J. Miller et al., Proceedings of the Workshop on Linear e^+e^- Colliders, Waikaloa, Hawaii, April 1993, eds. F.A. Harris et al. (World Scientific 1993), p. 577.
2. D.J. Miller and A. Vogt, Proceedings of the Workshop on e^+e^- Collisions at TeV Energies (Annecy, Gran Sasso, DESY 1995), ed. P. Zerwas (DESY 1996), p. 473;
   E. Accomando et al., Phys. Rep. 299 (1998) 1.
3. J. Chyla, `hep-ph/9811455`.
4. A. Gehrmann-De Ridder, `hep-ph/9906547` (these proceedings).
5. V. Budnev et al., Phys. Rep. 15C (1975) 181.
6. R. Nisius, `hep-ex/9907012` (these proceedings), and references therein.
7. I.F. Ginzburg et al., Nucl. Inst. Meth. A205 (1983) 47, A219 (1984) 5;
   V.I. Telnov, Nucl. Inst. Meth. A94 (1990) 72, `hep-ex/9908005` (these proceedings).
8. R. Brinkmann et al., Nucl. Instrum. Meth. A406 (1998) 13.
9. M. Glück, E. Reya and A. Vogt, Phys. Rev. D46 (1992) 1973.
10. J. Bümlein and A. Vogt, Phys. Rev. D58 (1998) 014020.
11. W.A. Bardeen and A.J. Buras, Phys. Rev. D20 (1979) 166, E: D21 (190) 2041;
    M. Fontannaz and E. Pilon, Phys. Rev. D45 (1992) 382, E: D46 (1992) 484;
    M. Glück, E. Reya and A. Vogt, Phys. Rev. D45 (1992) 3986.
12. L.E Gordon and J.K Storrow, Z. Phys. C56 (1992) 307, Nucl. Phys. B489 (1997) 405;
    P. Aurenche, M. Fontannaz and J.P. Guillet, Z. Phys. C64 (1994) 621;
    M. Glück, E. Reya and I. Schienbein, Phys. Rev. D60 (1999) 054019.
13. M. Glück, E. Reya and A. Vogt, Z. Phys. C53 (1992) 652.
14. W. R. Frazer, Phys. Lett. B194 (1987) 287.